Desalination and Water Treatment
www.deswater.com

doi: 10.5004/dwt.2023.30073

312 (2023) 132–138
November

Selective antimonite removal from water by montmorillonite-immobilized nanoscale zero-valent iron

Jinfeng Jiang[a,b], Shaokui Zheng[a,*], Bingyu Li[b], Xuan Fan[b], Hanjun Zhu[b], Ming Lei[b,*]

[a]*School of Environment, MOE Key Laboratory of Water and Sediment Sciences/State Key Lab of Water Environment Simulation, Beijing Normal University, Beijing 100875, China, emails: zsk@bnu.edu.cn (S. Zheng), 202121180085@mail.bnu.edu.cn (J. Jiang)*
[b]*College of Environment and Ecology, Hunan Agricultural University, Changsha 410128, China, emails: leiming@hunau.edu.cn (M. Lei), libingyu@hunau.edu.cn (B. Li), fanxuan@stu.hunau.edu.cn (X. Fan), 13170300949@163.com (H. Zhu)*

Received 14 July 2023; Accepted 3 October 2023

ABSTRACT

This study investigated the antimony (Sb) adsorption behavior on newly prepared montmorillonite (Mt)-immobilized nanoscale zero-valent iron (nZVI) (hereafter Mt-nZVI) in aqueous solution. Mt-nZVI showed the highest Sb adsorption capacity (71–76 mg·Sb·g^{-1} adsorbent) at pH 4–8. The pseudo-first-order and pseudo-second-order kinetic models fitted well (R^2 ³ 0.992) with the experimental data on Sb adsorption onto Mt-nZVI. The Langmuir isotherm model (R^2 = 0.99) was more suitable than the Freundlich isotherm model (R^2 = 0.95) for describing the adsorption of Sb on Mt-nZVI. Mt-nZVI had an almost 7 times higher theoretical Sb adsorption capacity than nZVI when calculated in terms of Fe. Neither 0.01 M phosphate nor 0.01 M sulfate had a significant effect the Sb adsorption capacity of Mt-nZVI, and more than 80% of the Sb adsorption capacity remained in the presence of 0.001–0.1 M NaCl or 1–30 mg·L^{-1} humic acid. However, the presence of 0.01 M silicate or carbonate or 0.0001 M arsenate significantly affected the Sb adsorption capacity of Mt-nZVI.

Keywords: Nanoscale zero-valent iron; Antimony; Adsorption

1. Introduction

Antimony (Sb) is widely used to produce pigments, batteries, catalysts for plastic synthesis, alloys for ammunition, additives in glassware and ceramics, semiconductors, and flame retardants in the construction industry [1,2]. As a toxic metalloid, however, exposure to Sb compounds can have serious human health effects, including acute (e.g., arrhythmia, Adams–Stokes syndrome, nerve injury, haematuria and spasm) and chronic illness (e.g., diarrhoea, headache, myalgia, rash, poor mental state, chest tightness, and abdominal colic) [3]. Therefore, Sb and its compounds have been defined as priority pollutants by the Council of the European Communities and the United States Environmental Protection Agency [1]. It is therefore necessary to develop efficient methods to control Sb discharge into the aqueous environment. Among the various treatment processes available, adsorption technology is the most commonly used due to its simplicity, treatment stability, and cost effectiveness [1,4]. In recent decades, there has been increasing interest in the use of nanoscale zero-valent iron (nZVI) for Sb removal from wastewater [1,5,6] due to its environmental friendliness, low production cost, high reactivity, and abundant reactive surface sites [7,8]. nZVI can form a bilayer structure with a metallic iron core and an outer iron oxide/(oxy) hydroxide (e.g., magnetite, maghemite, and goethite) shell [9,10]. It is well known that the precipitation, co-precipitation, redox and adsorption mechanisms contribute to the high contaminant removal capacities by this nanomaterial [10].

The main challenges to the use of nZVI for Sb removal involve the intrinsic characteristics of the nanoparticles

* Corresponding authors.

undergoing agglomeration [7,11], which often results in lower reactivity and poor mobility [7,9]. To overcome these problems, various supporting materials, including nanoscale magnetite [12], activated carbon [13], carbon nanotubes [1,14], biochar [3,15], granular polyvinyl alcohol [5], and various clay minerals, for example, montmorillonite (Mt) [7,9,16], kaolinite [17], zeolite [6,18], smectite [19], and bentonite (with Mt as the main component) [17,20,21], have been used to immobilize nZVI, to improve its treatment performance. Clay minerals are naturally available, nontoxic, low-cost, and environmentally friendly (i.e., biocompatible), and have a large surface area and high adsorption capability [7]. As a typical 2:1 layered silicate clay mineral [7], Mt consists of a central octahedral Al–O sheet between two tetrahedral Si–O sheets (i.e., a sandwich structure) [10,22], and its interlayer structure (0.1–0.8 nm thick) creates an ideal supporting matrix to disperse nZVI and hinder aggregation [7,22]. Mt-immobilized nZVI composite (hereafter Mt-nZVI) can improve the dispersion and mobility of nZVI, and reduce the particle size and oxidation tendency of nZVI while showing high contaminant removal efficiency [7]. However, little is known about the use of such materials for the removal of Sb from wastewater. Furthermore, an overall survey explores that there are insufficient studies comparing the Sb adsorption behavior on various nZVI composites.

This study was performed to investigate the Sb adsorption behavior on newly prepared Mt-nZVI in aqueous solution, including pH effects, adsorption kinetics, adsorption isotherms, and the effects of coexisting anions and natural organic matter. Based on these results, the Sb adsorption behavior on Mt-nZVI prepared in this study and other nZVI composites prepared in previous studies was fully compared, from which the potential effect of various supporting materials on the Sb removal performance by their nZVI composites was summarized.

2. Materials and methods

2.1. Materials and chemicals

Mt K10 (Sinopharm Chemical Reagent, Shanghai, China) was washed three times with deionized water, dried at 60°C in an electric drying oven (101-3AB; Tianjin Taisite Instrument Co., Ltd., Tianjin, China), and sieved through a 148 μm filter prior to use. Other chemical reagents, including chemically pure sodium alginate, guaranteed reagents (i.e., $KSbOC_4H_4O_6{\cdot}1/2H_2O$, HCl, and HNO_3 solutions) and analytical reagents (e.g., $NaBH_4$, absolute ethanol (99.7%), humic acid (HA), $FeSO_4{\cdot}7H_2O$, etc.) were also purchased from Sinopharm Chemical Reagent (Shanghai, China). Their solutions were prepared in deoxygenated deionized water (Milli-Q 18 MX; Millipore, Billerica, MA, USA), including 500 mg·L^{-1} Sb stock solution, and the pH was adjusted using 0.1 M NaOH or HCl solution with a pH meter (SevenCompact; Mettler Toledo, Greifensee, Switzerland).

2.2. Adsorbent preparation

Mt-nZVI was synthesized by liquid-phase reduction, as described previously [20] with minor modifications. Briefly, 1.6755 g of Mt K10 was dispersed in 100 mL of water in a 500-mL conical flask, ultrasonicated for 5 min, and stirred at 25°C ± 2°C for 15 min with a magnetic stirrer (MYP11-2; Shanghai Meiyingpu Instrument Manufacturing Co., Ltd., Shanghai, China) under a flow of nitrogen gas (4 L·min^{-1}). After adding 200 mL of $FeSO_4{\cdot}7H_2O$ solution (0.05 M) (i.e., Fe-to-Mt mass ratio of 1:3), the suspension was stirred for 60 min under nitrogen gas. Then, 100 mL of $NaBH_4$ solution (0.2 M) was dropped into the suspension and stirred under nitrogen gas for a further 10 min. Finally, 50 mL of sodium alginate solution (0.224 g·L^{-1}) was added and stirred under nitrogen gas for 10 min. The suspension was then sonicated by an ultrasonic cleaning machine (F-100P; Shenzhen Fuyang Technology Group Co., Ltd., Shenzhen, Guangdong, China), centrifuged (XiangYi L-530; Shanghai Huifen Electronic Technology Co., Ltd., Shanghai, China), and washed three times with deoxygenated absolute ethanol (99.7%). The resultant precipitate was dried at 60°C in a vacuum oven (DZ-2BCIV; Tianjin Taisite Instrument Co., Ltd., Tianjin, China) for 24 h. After grinding through a 148 μm filter with an agate mortar, the prepared material, designated as Mt-nZVI, was stored in sealed brown glass vials until use. Following the coating of Mt-nZVI on gold, its external surface morphology was examined by scanning electron microscopy (SEM) (Sigma 300; Zeiss, Oberkochen, Germany). Pure nZVI was also synthesized based on the procedure outlined above without the addition of clay and other chemicals, and the material without nZVI formation was used as a control in this study (designated as Mt).

2.3. Adsorption tests

Unless otherwise specified, all test solutions (50 mg·L^{-1} Sb, pH 5) were prepared by dissolution of $KSbOC_4H_4O_6{\cdot}1/2H_2O$ in 0.01 M NaCl solution, and the adsorption tests were conducted at 180 rpm and 25°C for 12 h in a water bath thermostatic oscillator (SHA-C; Changzhou Yate Experimental Instrument Co., Ltd., Changzhou, Jiangsu, China) with the addition of 0.04 g of adsorbent into 100-mL polypropylene bottles containing 100 mL of test solution. The polypropylene bottles were wrapped with aluminum foil to avoid photochemical reactions. Each run was conducted in triplicate under identical conditions. The Sb adsorption capacities were individually investigated at an initial pH of 3–9 for 24 h, or in test solution containing 100 mg·L^{-1} Sb for adsorption kinetics, or in various test solutions containing 10–300 mg·L^{-1} Sb for adsorption isotherms, or in various test solutions in the presence of 0–0.1 M Cl^-, 0–30 mg·L^{-1} HA, or 0.01 M silicate, phosphate, carbonate, sulfate, or 0.0001 M arsenate. When final equilibrium was reached, samples of 8 mL of the suspension were withdrawn and immediately filtered using syringe filters (0.22 μm) for measurement. The Sb concentrations in the filtrates were determined by inductively coupled plasma optical emission spectroscopy (Optima 8300; PerkinElmer, Waltham, MA, USA). Three replicates were employed for each analysis.

The amount of adsorbed Sb at time t (q_t, expressed as mg·Sb·g^{-1} adsorbent) and the Sb adsorption capacity at equilibrium (q_e, expressed as mg·Sb·g^{-1} adsorbent) were calculated according to the following equations:

$$q_t = \frac{\left(C_0 - C_t\right)V}{m} \quad (1)$$

where C_0 and C_t (mg·L^{-1}) are the initial Sb concentration and the value at time t (or C_e at equilibrium), respectively, and V is the volume of the test solution (L).

In this study, equilibrium was described by Langmuir and Freundlich isotherm models:

$$q_e = \frac{q_m K_L C_e}{1 + K_L C_e} \tag{2}$$

$$q_e = K_F C_e^{1/n} \tag{3}$$

where q_m is the maximum sorption capacity (mg·g^{-1}) and K_L is the Langmuir constant (L·mg^{-1}); K_F is the Freundlich constant (L·mg^{-1}) and $1/n$ is the intensity of heterogeneity.

During the kinetic experiments of Mt-nZVI adsorption, aliquots of 2 mL of the suspensions were withdrawn for measurement at designed time intervals. The mass transfer efficiency between Mt-nZVI and Sb were evaluated by pseudo-first-order and pseudo-second-order kinetic models [9]:

$$q_t = q_e\left(1 - \exp\left(-k_1 t\right)\right) \tag{4}$$

$$\frac{dq_t}{dt} = k_2\left(q_e - q_t\right)^2 \tag{5}$$

where q_t is the amount of adsorbed Sb at different contact times t (mg·g^{-1}), and k_1 (min^{-1}) and k_2 (g·mg^{-1}·h^{-1}) represent the adsorption rate constants of the respective kinetic models.

3. Results and discussion

Generally, pristine spherical nZVI undergoes agglomeration to form chain-like aggregates [22]. However, its three-dimensional growth is markedly limited when interacting with clay minerals, often resulting in a smaller size in Mt-nZVI [10,22]. In this study, the microstructure and morphology of freshly prepared Mt-nZVI were characterized by SEM (Fig. 1). As reported previously [22], the abundant nZVI beads were homogeneously distributed on the surface of the Mt sheets in this study (Fig. 1), demonstrating that the presence of Mt effectively prevented agglomeration of nZVI [22]. A very small amount of nZVI remained in the form of short chains or small aggregates in previous Mt-nZVI samples [22], however, no such residue was observed in this study. Based on a preliminary test (data not shown), 0.04 g of Mt-nZVI was added to the test solutions to simultaneously optimize operational costs and treatment performance (data not shown). Additionally, all Sb adsorption tests in this study were evaluated in terms of highly toxic Sb(III).

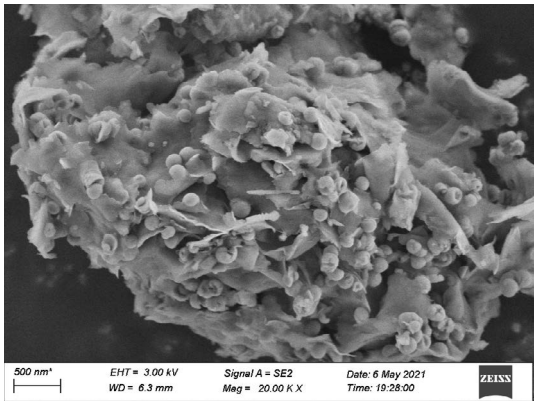

Fig. 1. Scanning electron microscopy image of Mt-nZVI.

3.1. Effects of initial pH on Sb adsorption

In this study, the effects of initial pH (pH 3–9) on Sb adsorption capacities of Mt-nZVI, nZVI, and Mt were investigated, and the results are shown in Fig. 2. By contrast, nZVI showed higher Sb adsorption capacity (81–106 mg·Sb·g^{-1} adsorbent) than Mt-nZVI (45–76 mg·Sb·g^{-1} adsorbent), while Mt showed negligible adsorption (2.0–3.5 mg·Sb·g^{-1} adsorbent) at initial pH 3–9. Therefore, the Sb adsorption capacity of Mt-nZVI was mainly attributable to that of nZVI rather than other components, and the lower Sb adsorption capacity of Mt-nZVI compared to nZVI should be attributable to the smaller amount of nZVI in Mt-nZVI at identical adsorbent dosage.

Similar to adsorption of arsenic onto Mt-nZVI [10], the interaction between Sb(III) and nZVI (or Mt-nZVI) may be predominantly attributable to a chemical mechanism, that is, ligand exchange independent of pH [10], leading to efficient Sb adsorption over a wide initial pH range in this study. It is well known that nZVI effectively adsorbs Sb(III) in aqueous solution by its oxidation to Sb(V) and subsequent complex Sb(III)/Sb(V) surface adsorption [12,14,15]. While the neutral trihydroxy molecules (e.g., $Sb(OH)_3$) are the dominant Sb(III) species in aqueous solution at pH 3–11, anions (e.g., $Sb(OH)_6^-$) are the dominant Sb(V) species in aqueous solution at pH 4–10 [1,5]. On the other hand, when pristine nZVI has an isoelectric point or zero point charge (pH_{PZC}) of 7.8 [14], different supporting materials were reported to generate markedly different pH_{PZC} of nZVI composites, for example, pH 3.7 for zeolite-immobilized nZVI [6], 7.5 for carbon nanotube-immobilized nZVI [1], 6.5–6.8 for granular polyvinyl alcohol-immobilized nZVI

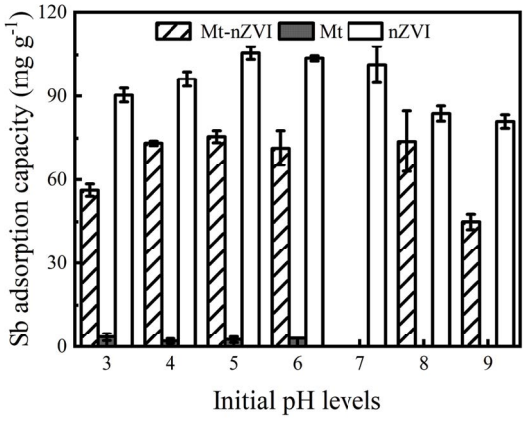

Fig. 2. Effect of initial pH on the Sb adsorption capacities of Mt-nZVI, Mt and nZVI. Error bars correspond to the standard deviations of duplicate analyses.

[5], and 8.2 for Mt-nZVI [9]. Under the conditions, solution pH is a key parameter affecting both the surface properties of Mt-nZVI (e.g., the surface equipotential point, iron species) [7] and the predominant Sb oxyanionic species/charges [1,5], finally affecting the Sb adsorption capacity. For example, the positively charged nZVI could electrostatically attract negatively charged Sb(V) at pH < pH_{ZPC} [5,9]. Lower Sb adsorption at high pH should be attributable to electrostatic repulsion resulting from the electronegative adsorbent surface or the potential nZVI passivation effect [1]. Similar pH dependent of Sb adsorption performance has been documented previously for nZVI composites immobilized on other supporting materials [1,5,12]. However, there were marked differences in optimal pH range for maximum Sb adsorption on various nZVI composites, for example, pH 3–11 for nanoscale magnetite-immobilized nZVI [12], pH < 5 for activated carbon-immobilized nZVI [13] or granular polyvinyl alcohol-immobilized nZVI [5], and pH 5–8 (or 5–6) for carbon nanotube-immobilized nZVI [1]. In this study, Mt-nZVI showed the highest Sb adsorption capacity at pH 4–8 (71–76 mg·Sb·g^{-1} adsorbent) in Fig. 2.

3.2. Sb adsorption kinetics

Adsorption kinetics can be used to assess the potential of adsorbents for practical application, as the fast adsorption process can reduce the cost of the adsorbent [15]. Fig. 3 shows the time profiles of the amounts of Sb adsorbed on Mt-nZVI over 12 h. A sharp increase in the amount of adsorbed Sb from 0 to 106 mg·Sb·g^{-1} adsorbent was observed within the first 2 h, likely attributable to Sb-Fe coprecipitation after nZVI was corroded, generating large amounts of hydroxyl and dissolved iron [24]. Subsequently, the adsorbed Sb amount varied within a narrow range of 132–136 mg·Sb·g^{-1}, over 6–12 h, suggesting that adsorption saturation was achieved after 6 h. The time required to achieve equilibrium using Mt-nZVI was slightly longer than that on carbon nanotube-immobilized nZVI (4 h) [1], but much shorter than for nZVI composites immobilized on other supporting materials, for example, 48 h for granular polyvinyl alcohol-immobilized nZVI [5].

In this study, the pseudo-first-order and pseudo-second-order kinetic models were used to fit the experiment data. To check the validation of both kinetic models visually, their theoretical lines are also shown in Fig. 3. Generally, the pseudo-first-order kinetic model assumes that adsorption is governed by the diffusion steps, while the pseudo-second-order kinetic model assumes that adsorption rates are controlled by chemisorption and involve the sharing or transfer of electron pairs between the adsorbate and the adsorbent [15]. In this study, both kinetic models fitted well with the experimental data on Sb adsorption onto Mt-nZVI (R^2 = 0.992 or 0.994). In previous studies, the Sb adsorption on nZVI [24] or its composites immobilized on other supporting materials, such as biochar [3], carbon nanotubes [1], nanoscale magnetite [12], or granular polyvinyl alcohol [5], could often be more effectively presented by the pseudo-second-order kinetic model. Zhou et al. [6] reported that the pseudo-second-order or pseudo-first-order model described more accurately the adsorption of Sb by nZVI-zeolite at a zeolite-nZVI dosage of 1 or 2 g·L^{-1} [6]. Such differences, including adsorbent dosage, may explain differences in Sb adsorption behavior among these studies.

3.3. Sb adsorption isotherms

Fig. 4 presents a quantitative comparison of the equilibrium Sb concentration and adsorption capacities on Mt-nZVI and nZVI with varied initial Sb concentrations (10–300 mg·L^{-1}). Langmuir and Freundlich isotherm models were used to fit these experiment data, and their model parameters were calculated and were presented in Table 1. The calculated lines using these two model parameters are also shown in Fig. 4. While the Langmuir model assumes monolayer adsorption onto the homogeneous adsorbent surface with a finite number of identical sites [23], the Freundlich model is empirical in nature and allows multilayer adsorption [9]. In this study, the Langmuir isotherm model (R^2 = 0.99) was more suitable than the Freundlich isotherm model (R^2 = 0.95) for describing the adsorption of Sb on Mt-nZVI, similar to Sb adsorption on nanoscale magnetite-immobilized nZVI [12] or granular polyvinyl alcohol-immobilized nZVI [5], or the adsorption of other heavy metals on Mt-nZVI [7]. The different supporting materials

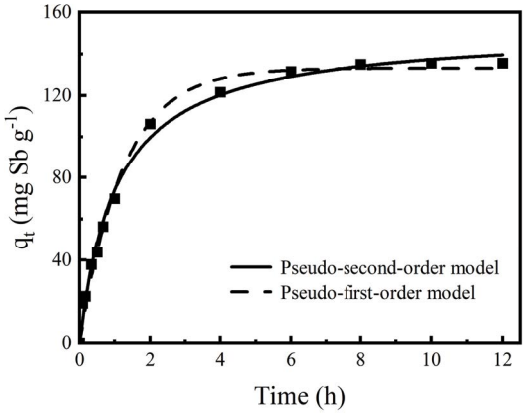

Fig. 3. Time profiles of the amounts of Sb adsorbed on Mt-nZVI over 12 h.

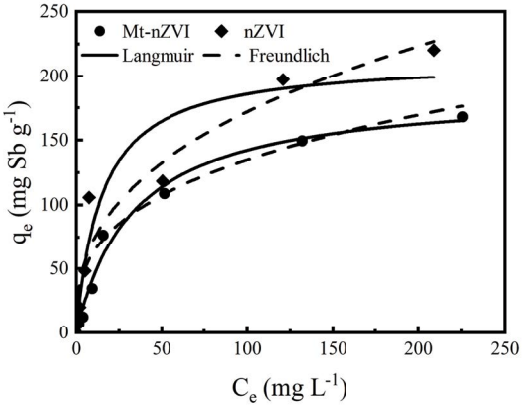

Fig. 4. Adsorption isotherm of Sb on Mt-nZVI and nZVI.

Table 1
Langmuir and Freundlich model isotherm parameters for Sb adsorption on Mt-nZVI and nZVI

Adsorbents	Langmuir model			Freundlich model		
	q_m (mg·g^{-1})	K_L (L·mg^{-1})	R^2	K_F	n	R^2
Mt-nZVI	189	0.030	0.99	29	3.02	0.95
nZVI	213	0.068	0.92	30	2.66	0.95

may also result in the different applicability of two adsorption isotherms. For example, the Freundlich model better fitted the adsorption of Sb(III) on zeolite-nZVI [6].

Based on the Langmuir model parameter q_m in Table 1, Mt-nZVI exhibited significantly higher theoretical (i.e., the maximum) Sb adsorption capacity (189 mg·Sb·g^{-1} adsorbent) than previous nZVI composites immobilized on nanoscale magnetite (88 mg·Sb·g^{-1} adsorbent) [12], zeolite (135 mg·Sb·g^{-1} adsorbent) [6], carbon nanotube (75 mg·Sb·g^{-1} adsorbent) [14], and biochar (160 mg·Sb·g^{-1} adsorbent) [3]. In this study, the theoretical Sb adsorption capacity of Mt-nZVI was 11% lower than that of nZVI. However, the theoretical Sb adsorption capacity of Mt-nZVI was almost 7 times that of nZVI when calculated in terms of nZVI (i.e., 16.4 vs. 2.4 mg·Sb·mol^{-1} Fe, respectively). In other words, the dispersal and immobilization of nZVI onto Mt markedly enhanced the Sb adsorption capacity of nZVI.

3.4. Effects of coexisting anions and natural organic matter

Anions and natural organic matter present in water/wastewater may compete for adsorption sites and finally decrease the adsorbent capacity of nZVI composites immobilized on various supporting materials [3,5]. Furthermore, the choice of supporting material can also influence Sb adsorption performance of the resulting nZVI composites in the presence of coexisting anions and natural organic matter. For example, Sb adsorption behavior of granular polyvinyl alcohol-immobilized nZVI in the presence of coexisting anions or natural organic matter decreased in the order arsenate > phosphate > silicate > sulfate > nitrate > chloride [5], that of carbon nanotube-immobilized nZVI decreased in the order phosphate > silicate > arsenate > sulfate, nitrate > chloride, HA [1], and that of biochar-immobilized nZVI decreased in the order phosphate > silicate > chloride > carbonate > sulfate [3]. Therefore, we further investigated the potential effects of ionic strength or HA concentration and coexisting anions (e.g., chloride, silicate, phosphate, carbonate, sulfate, and arsenate) on the Sb adsorption capacity of Mt-nZVI (Fig. 5).

3.4.1. Effects of ionic strength or HA concentration

The potential effects of inorganic ionic strength on Mt-nZVI adsorption capacity were often investigated at low salinity levels in previous studies, for example, 0.001–0.1 M $NaNO_3$ during U(VI) adsorption [16] or 0.001–0.05 M NaCl during Cr(VI) adsorption [21]. In this study, the potential effects of coexisting 0.001–0.1 M NaCl or 1–30 mg·L^{-1} HA on the Sb adsorption capacity of Mt-nZVI are shown in Fig. 5a and b. It was reported that 0.001–0.1 M $NaNO_3$ had

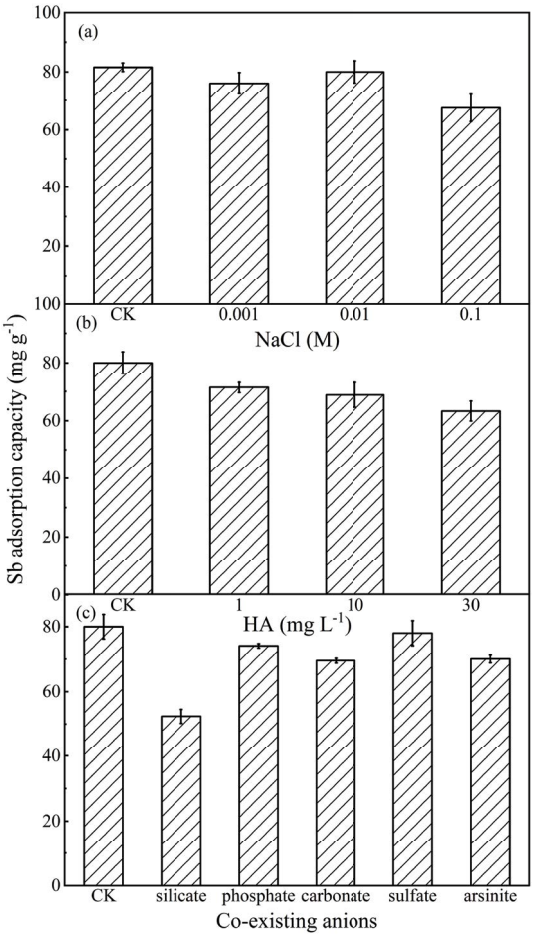

Fig. 5. Effect of various ionic strengths (a), humic acid concentrations (b), or co-existing anions (c) on the Sb adsorption capacity of Mt-nZVI.

no significant effect on U(VI) adsorption on Mt-nZVI [16], while increased NaCl concentration (0.001–0.05 M) enhanced Cr(VI) adsorption on bentonite-immobilized nZVI [21]. In this study, 0.001–0.1 M NaCl showed a significant effect on the Sb adsorption capacity of Mt-nZVI in comparison with the control ($P \leq 0.04$), with the maximal reduction of 17% at 0.1 M NaCl. In previous studies, coexisting 10 mg·L^{-1} dissolved natural organic matters significantly reduced Sb removal from 90% to 72% by carbon nanotube-immobilized nZVI [14], while ≥10 mg·L^{-1} HA significantly reduced the Sb adsorption capacity on biochar-immobilized nZVI [3]. Similarly, 1–30 mg·L^{-1} HA significantly ($P < 0.05$) reduced the Sb adsorption capacity on Mt-nZVI. The Sb adsorption capacity decreased with increasing HA concentration, with a maximal reduction of 21% (Fig. 5b). This can be explained by the large molecular weight of HA, which can block surface sites, and its ability to chelate these sites [3]. Although 0.001–0.1 M NaCl or 1–30 mg·L^{-1} HA significantly inhibited Sb adsorption on Mt-nZVI, at least 79% of the Sb adsorption capacity remained at 0.1 M NaCl or 30 mg·L^{-1} HA. The highest ionic strength and HA concentration selected in this study were much higher than those in the actual environment, and so their impacts could be lower in actual water samples.

3.4.2. Effects of coexisting anions

In many cases, stronger inhibitory effects on Sb adsorption on nZVI composites were observed in the presence of coexisting phosphate, silicate [1,3], and arsenate [1] due to their chemical similarity to Sb oxyanions [1,3] and, therefore, similar mechanism of adsorption to Fe [14]. In particular, P, As, and Sb are located in the same main group in the periodic table. In this study, as shown in Fig. 5c, coexisting phosphate (P = 0.094) and sulfate (P = 0.621) had no significant effect on the Sb adsorption capacity of Mt-nZVI, while coexisting silicate (P = 0.001), carbonate (P = 0.018), and arsenate (P = 0.024) significantly influenced the Sb adsorption capacity. The significant inhibition of Sb adsorption performance on nZVI composites was also observed in the presence of specific concentrations of anions, for example, ≥500 mg·L^{-1} chloride or sulfate, ≥50 mg·L^{-1} nitrate, and ≥5 mg·L^{-1} arsenate or phosphate on granular polyvinyl alcohol-immobilized nZVI [5], and ≥0.01 M silicate on carbon nanotube-immobilized nZVI [14]. Mt-nZVI seems to adsorb Sb effectively in the presence of a higher phosphate level (~970 mg·L^{-1}) than granular polyvinyl alcohol-immobilized nZVI. The presence of 0.01 M silicate resulted in the maximum decrease in Sb adsorption capacity, by 35%, in this study. However, with silicate, a concentration of 761 mg·L^{-1} is almost never encountered with Sb in environmental samples. Therefore, its adverse effect at such levels does not seriously limit the application of Mt-nZVI.

In many cases, various heavy metals often coexisted in aquatic environments and should be simultaneously removed to the discharge limits [10,23]. There have been a number of previous studies regarding the elimination of other heavy metals, such as As(III) and As(V) [9], Se(V) [10], Pb(II), Zn(II), Cu(II), and U(VI) [7], and Cr(VI) [7,22] by Mt-nZVI. The results presented here further expanded the potential applications of Mt-nZVI in the efficient and selective removal of coexisting heavy metals from the environment under extreme conditions. In the near future, a fixed-bed system filled with Mt-nZVI will be designed to continuously treat industrial wastewater containing Sb and other heavy metals on the basis of the process parameters optimized in this study. The techno-economic assessment of the fixed-bed system will be conducted in order to provide an overall information for its practical application.

4. Conclusion

The Sb adsorption capacity of Mt-nZVI was mainly attributable to that of nZVI rather than other components. The supporting material type significantly influenced the optimum pH range to achieve the highest Sb adsorption capacity by nZVI composites. As compared with other nZVI composites, the time required to reach equilibrium was much shorter when Mt-nZVI was used (except carbon nanotube-immobilized nZVI). Furthermore, Mt-nZVI exhibited significantly higher theoretical Sb adsorption capacity than previous nZVI composites. Mt as a supporting material expanded the potential applications of nZVI in the removal of various heavy metals, including Sb, from the environment under extreme conditions.

Acknowledgment

This work was supported by the National Natural Science Foundation of China (No. 22176015 and 51878050).

Disclosure statement

No potential conflict of interest was reported by the authors.

References

[1] S. Mishra, J. Dwivedi, A. Kumar, N. Sankararamakrishnan, Removal of antimonite (Sb(III)) and antimonate (Sb(V)) using zerovalent iron decorated functionalized carbon nanotubes, RSC Adv., 6 (2016) 95865–95878.
[2] T. Huang, L.F. Liu, J.J. Xu, S.W. Zhang, Combination of electrokinetics and nano zero-valent iron-based adsorption enhances Sb(V) removal from feed water in the batch and column mode processes, Desal. Water Treat., 150 (2019) 166–191.
[3] D.N. Wei, B.Y. Li, L. Luo, Y.X. Zheng, L.H. Huang, J.C. Zhang, Y. Yang, H.L. Huang, Simultaneous adsorption and oxidation of antimonite onto nano zero-valent iron sludge-based biochar: indispensable role of reactive oxygen species and redox-active moieties, J. Hazard. Mater., 391 (2020) 122057, doi: 10.1016/j.jhazmat.2020.122057.
[4] M.T. Sikder, R. Kubota, M. Akter, M.M. Rahman, K.F.B. Hossain, M.S. Rahaman, S. Banik, T. Hosokawa, T. Saito, M. Kurasaki, Adsorption mechanism of Cu(II) in water environment using chitosan-nano zero valent iron-activated carbon composite beads, Desal. Water Treat., 145 (2019) 202–210.
[5] X.Q. Zhao, X.M. Dou, D. Mohan, C.U. Pittman, Y.S. Ok, X. Jin, Antimonate and antimonite adsorption by a polyvinyl alcohol-stabilized granular adsorbent containing nanoscale zero-valent iron, Chem. Eng. J., 247 (2014) 250–257.
[6] Z. Zhou, C.M. Dai, X.F. Zhou, J.F. Zhao, Y.L. Zhang, The removal of antimony by novel nZVI-zeolite: the role of iron transformation, Water Air Soil Pollut., 226 (2015) 76, doi: 10.1007/s11270-014-2293-2.
[7] Y. Yin, W. Zheng, A. Yan, C. Zhang, Y. Gou, C. Shen, A review on montmorillonite-supported nanoscale zerovalent iron for contaminant removal from water and soil, Adsorpt. Sci. Technol., 2021 (2021) 9340362, doi: 10.1155/2021/9340362.
[8] S. Padungthon, A. Pranudta, M.M. El-Moselhy, P. Kidkhunthod, P. Amonpattaratkit, P. Jiemvarangkul, The capability of nanoscale zero valent iron particles for removal of concentrated lead in spent acidic regeneration solution, Desal. Water Treat., 194 (2020) 160–171.
[9] S. Bhowmick, S. Chakraborty, P. Mondal, W. Van Renterghem, S. Van den Berghe, G. Roman-Ross, D. Chatterjee, M. Iglesias, Montmorillonite-supported nanoscale zero-valent iron for removal of arsenic from aqueous solution: kinetics and mechanism, Chem. Eng. J., 243 (2014) 14–23.
[10] J. Suazo-Hernandez, K. Manquian-Cerda, M. de la Luz Mora, M. Molina-Roco, M. Angelica Rubio, B. Sarkar, N. Bolan, N. Arancibia-Miranda, Efficient and selective removal of Se^{VI} and As^{V} mixed contaminants from aqueous media by montmorillonite-nanoscale zero valent iron nanocomposite, J. Hazard. Mater., 403 (2021) 123639, doi: 10.1016/j.jhazmat.2020.123639.
[11] D. Chauhan, J. Dwivedi, N. Sankararamakrishnan, Novel chitosan/PVA/zerovalent iron biopolymeric nanofibers with enhanced arsenic removal applications, Environ. Sci. Pollut. Res., 21 (2014) 9430–9442.
[12] W.B. Li, F.L. Fu, Z.C. Ding, B. Tang, Zero valent iron as an electron transfer agent in a reaction system based on zero valent iron/magnetite nanocomposites for adsorption and oxidation of Sb(III), J. Taiwan Inst. Chem. Eng., 85 (2018) 155–164.
[13] H.J. Zhu, Q. Huang, M.Y. Shi, S. Fu, X.J. Zhang, Z. Yang, J.H. Lu, B. Liu, Adsorption of Sb(III) from aqueous solution by nZVI/

AC: a magnetic fixed-bed column study, Nanomaterials, 11 (2021) 1912, doi: 10.3390/nano11081912.
[14] F.Q. Liu, Y.B. Liu, N. Ding, S.N. Yang, C.S. Shen, F. Li, W. Sand, An affordable carbon nanotube filter functionalized with nanoscale zerovalent iron for one-step Sb(III) decontamination, Environ. Eng. Sci., 37 (2020) 490–496.
[15] J.H. Ji, S.Q. Xu, Z.Q. Ma, Y.Z. Mou, Optimisation of preparation conditions and removal mechanism for trivalent antimony by biochar-supported nano zero-valent iron, Environ. Technol. Innovation, 26 (2022) 102240, doi: 10.1016/j.eti.2021.102240.
[16] J. Xu, Y. Li, C. Jing, H. Zhang, Y. Ning, Removal of uranium from aqueous solution using montmorillonite-supported nanoscale zero-valent iron, J. Radioanal. Nucl. Chem., 299 (2014) 329–336.
[17] D.D. Tomasevic, G. Kozma, D.V. Kerkez, B.D. Dalmacija, M.B. Dalmacija, M.R. Becelic-Tomin, A. Kukovecz, Z. Konya, S. Roncevic, Toxic metal immobilization in contaminated sediment using bentonite- and kaolinite-supported nano zero-valent iron, J. Nanopart. Res., 16 (2014) 2548, doi: 10.1007/s11051-014-2548-2.
[18] N. Arancibia-Miranda, S.E. Baltazar, A. Garcia, D. Munoz-Lira, P. Sepulveda, M.A. Rubio, D. Altbir, Nanoscale zero valent supported by zeolite and montmorillonite: template effect of the removal of lead ion from an aqueous solution, J. Hazard. Mater., 301 (2016) 371–380.
[19] K.A. Uz-Zaman, B. Biswas, M.M. Rahman, R. Naidu, Smectite-supported chain of iron nanoparticle beads for efficient clean-up of arsenate contaminated water, J. Hazard. Mater., 407 (2021) 124396, doi: 10.1016/j.jhazmat.2020.124396.
[20] M.Y. Zhang, K.X. Yi, X.W. Zhang, P. Han, W. Liu, M.P. Tong, Modification of zero valent iron nanoparticles by sodium alginate and bentonite: enhanced transport, effective hexavalent chromium removal and reduced bacterial toxicity, J. Hazard. Mater., 388 (2020) 121822, doi: 10.1016/j.jhazmat.2019.121822.
[21] A. Soliemanzadeh, M. Fekri, The application of green tea extract to prepare bentonite-supported nanoscale zero-valent iron and its performance on removal of Cr(VI): effect of relative parameters and soil experiments, Microporous Mesoporous Mater., 239 (2017) 60–69.
[22] Y.Y. Zhang, H. Jiang, Y. Zhang, J.F. Xie, The dispersity-dependent interaction between montmorillonite supported nZVI and Cr(VI) in aqueous solution, Chem. Eng. J., 229 (2013) 412–419.
[23] A. Hamdy, M.K. Mostafa, M. Nasr, Techno-economic estimation of electroplating wastewater treatment using zero-valent iron nanoparticles: batch optimization, continuous feed, and scaling up studies, Environ. Sci. Pollut. Res., 26 (2019) 25372–25385.
[24] C.M. Dai, Z. Zhou, X.F. Zhou, Y.L. Zhang, Removal of Sb(III) and Sb(V) from aqueous solutions using nZVI, Water Air Soil Pollut., 225 (2014) 1799, doi: 10.1007/s11270-013-1799-3.